Civil Engineering and Applied Solutions

Research Article

journal homepage: ceas.journals.umz.ac.ir

CEAS Civil Engineering and Applied Solutions

Experimental Assessment for Restoring the Flexural Strength of Severely Damaged RC Beams Using NSM Steel Bars and External Confinement

Rasha A. Aljazaari [a], Javad Vaseghi Amiri [b*], Hayder Alghazali [a]

[a] *Department of Civil Engineering, Engineering College/ Kufa University, Najaf, Iraq*
[b] *Department of Civil Engineering, Babol Noshirvani University of Technology, Babol, Iran*

A R T I C L E I N F O

Article history:

Received 15 April 2026

Revised 03 May 2026

Accepted 10 June 2026

Available online 01 January 2027

Keywords:

Repairing

Near-surface mounting (NSM)

Hooked bar configuration

Epoxy

Cementitious material

External bonding

A B S T R A C T

Reinforced concrete beams may require repair to regain lost capacity due to unforeseen events, such as accidents or loading exceeding the limits that weren't predicted in the design. The purpose of this research is to restore the load capacity of RC beams after severe mid-span damage. Eight reinforced concrete beams were utilized in this study. A near-surface mounting (NSM) technique was examined, with various variables including the configuration of repair bars, adhesive materials, diameter of repair bars, as well as externally bonded repair with a steel plate in the damaged zone. The result revealed that straight bars restored up to 94.5% of ultimate strength, while hooked bars slightly exceeded the control by 5%. Epoxy bonds achieved up to 105.6% recovery, surpassing cementitious systems that ranged from 66.8% to 110.6%. Larger repairing bars of 16 mm restored capacities up to 115.6%, significantly higher than the recovery range from 66.8% to 82.4% for 12 mm bars. Confinement raised the ultimate load marginally above control, of 5.4%, while unconfined beams recovered only 82.4%. Cementitious adhesives offered an economical repair option for moderate-demand applications; however, both bonding systems reduced ductility by up to 55.6% and energy absorption by up to 89.3%. Straight bars improved stiffness and ductility compared with hooked bars, while larger bar diameters of 16 mm reduced performance losses and enhanced stiffness. Confinement improved service stiffness and partially limited energy-absorption losses, although ductility remained below that of the control beam.

How to cite this article: Aljazaari, R.A. Vaseghi Amiri, J. Alghazali, H. Experimental Assessment for Restoring the Flexural Strength of Severely Damaged RC Beams Using NSM Steel Bars and External Confinement .Civil Engineering and Applied Solutions. 2027; 3(1): 161–178. doi:10.22080/ceas.2026.31548.1090.

1. Introduction

The structural components experience higher service loads or deformations than their design capacity due to overloads or changes in function, leading to cracks induced through insufficient ultimate strength [1]. Bridges are a common example of a bridge girder failing locally due to excessive use, overloading, failure to follow height specifications for each bridge, and various other reasons [2]. During the initial design, these considerations were not taken into account, which contributed to stress exceeding their capacity [3].

In general, repairing damaged concrete structures is essential not only to ensure they function as intended during their expected service trajectory but also to guarantee the safety and functionality of related components so that they meet the precise requirements of modern and future structures [4]. A good repair boosts the function and performance of structures, restoring and increasing their strength and stiffness. In fact, repairing techniques, rather than replacing structures, have become both efficient and more economically beneficial. Maintaining structural elements tends to be cheaper and faster than reconstructing them [5, 6]. Generally,

* Corresponding author.
E-mail addresses: vaseghi@nit.ac.ir (J. Vaseghi Amiri).

https://doi.org/10.22080/ceas.2026.31548.1090
ISSN: 3092-7749/© 2027 The Author(s). Published by University of Mazandaran.

repair is seen as a process where the behavior of the concrete element after repair does not deviate much from its original behavior. Its main goal is to restore the architectural shape and function of the concrete structure without significantly enhancing its performance [7]. In the current economic environment, repairing concrete structures that were damaged to comply with the stricter restrictions regarding the maximum strength and serviceability of the latest codes, as well as repairing preexisting concrete constructions to support more allowable loads, appear to be more viable options compared to demolition and building from scratch [8].

A variety of new and complex repair materials and procedures have been successfully developed to improve the functionality and performance of damaged reinforced concrete structures. The two traditional methods are the NSM method and bonding by steel plate [9, 10]. The NSM was the more effective approach and was also easier and faster to use, ensuring fewer fragile failure modes. Rods or strips can be used to perform this technique [11]. In Near-surface-mounted (NSM) systems, the embedded bars or plates are installed into premade grooves on the concrete surface; bonding between the bar and the grooves can be achieved using a suitable adhesive cured in place. In NSM systems, the groove dimensions should be a minimum of 1.5 times the diameter of the embedded bar. The clear groove spacing, which is at least twice the groove depth of the NSM system, should be used to prevent overlapping tensile stresses around the embedded bars. Additionally, a clear edge space of four times the groove depth of the NSM must be provided to reduce the influence of debonding-type failures at the edge [12].

NSM offers many privileges over the (EB) approach, such as protection, enhanced bonding, good appearance, and surface prepping. The bond quality has improved significantly over the EB method; it remains the key consideration for designing elements strengthened or repaired in the NSM method [13]. NSM is also superior to EBR because it has a more even distribution of strain, which maximizes strain utilization and provides greater resistance to environmental influences, as it is plumbed beneath the surface of the concrete. Sometimes, the embedded rods are placed under grout, which means the visual effect of the NSM technique is almost imperceptible. For parking lot slabs experiencing low negative moment levels, embedded bars in the NSM approach are used to enhance the structure's capacity, as the surface cuts shield the embedded bars from the effects of vehicular traffic. According to the NSM approach, bar installation requires less work since treating pre-existing concrete surfaces is unnecessary. Surface non-regularity or weakened cover of concrete no longer presents an issue, given that the drilled cuts for embedded bars for the NSM method have been profound and narrow [14].

Some researchers evaluated the NSM using steel rods. Rahman et al. [15] examined the flexural behavior of RC beams strengthened using NSM steel bars and confirmed that this technique is a cost-effective solution for enhancing flexural performance. In addition, cement mortar was verified to perform nearly as well as using 100% epoxy adhesive when partially replaced by 50% epoxy glue in the NSM groove. The NSM technique outperformed the plate bonding method, requiring only one-third of the steel, thereby highlighting its efficiency and economic potential for retrofitting applications. Mobin and Haque [16] evaluated the performance of the NSM with steel bars, demonstrating that doubling the amount of NSM steel reinforcement raised the maximum load by 102.4%, offered a high level of ductility, and resulted in a ductile failure mechanism. The employment of cement paste instead of epoxy adhesive exhibits adequate strength and ductility, significantly reducing costs with only a minor decrease in performance. Sabah and Hamza [17] evaluated the effectiveness of the NSM technique using steel rebars. The outcomes revealed that NSM steel bars increased the ultimate load by 28.5% and ductility by 24.6%. Kholil et al. [18] employed finite element analysis to examine the flexural repair of RC beams using the NSM-steel bars technique, demonstrating that providing 80% NSM reinforcement to the tensile zone improved the ultimate load by approximately 1.64 times and enhanced stiffness by 2.24 times.

Other papers have studied the use of a steel plate as an external strengthening or repair method. Olajumoke and Dundu [19] reviewed various techniques for strengthening RC elements in bending. They highlighted the effectiveness of steel plates in enhancing flexural strength through both Externally Bonded Reinforcement (EBR) and NSM methods. While both methods are effective, the study found that EBR offers better practical applicability than NSM in real-world scenarios. Abuodeh et al. [20] experimentally evaluated the performance of RC beams strengthened using externally bonded and bolted Aluminum Alloy (AA) plates. Beams with bonded AA plates increased capacity by 32% and deflection by 45%, whereas those with both bolting and bonding increased capacity by 24% and deflection by 84%. In conclusion, combining bolting and bonding significantly enhances ductility and reduces debonding, resulting in an effective anchorage solution with minimal loss of strength. Zhang et al. [21] introduced a new steel plate strengthening technique for damaged RC beams. The strengthened beams exhibited an increase in cracking moments from 214.5% to 271.5%, and a bearing capacity boost of 53.1% to 73.7%. The primary failure mode was interface peeling. Moreover, the flexural stiffness nearly doubled on average, and further increasing the steel plate thickness improved both stiffness and strain performance.

While prior research has examined NSM strengthening approaches, limited attention has been devoted to the repair of severely damaged lap-spliced reinforced concrete (RC) beams using NSM steel bars. Additionally, the comprehensive assessment of hook-bar configuration, epoxy versus cementitious adhesives, and external confinement remains insufficiently explored. Consequently, this study aims to address these research gaps through a systematic experimental program.

2. Research significant

The research highlights practical, evidence-based solutions for repairing damaged RC beams, showing how repair combinations restore performance and improve serviceability. It emphasizes the importance of bar configuration and steel plate confinement in stress distribution and ductility. Advocating for repair over replacement, the study supports sustainable, cost-effective practices that extend the lifespan of structures and deepen the understanding of material-structure interactions, guiding more effective restoration techniques.

3. Research obejectives

Accordingly, the objectives of the present study are summarized as follows:

1. To investigate the effect of repair bar configuration (straight versus hooked bars) on the behavior of severely damaged RC beams repaired using the NSM technique.
2. To evaluate the influence of bonding material type (epoxy versus cementitious adhesive) on repair effectiveness.
3. To examine the effect of repair bar diameter on the flexural response of repaired beams.
4. To assess the contribution of external steel plate confinement to the performance of the proposed repair system.
5. To evaluate the effectiveness of the previous parameters based on the recorded and calculated response metrics, namely ultimate load capacity (Pu), ductility index (μ), stiffness, and energy absorption, in order to identify the most efficient and practical repair strategy.

4. Experimental work

4.1. Specimens details

Eight reinforced concrete beam specimens with rectangular cross-sections, measuring 200 mm in width and 300 mm in depth, with a total length equal to 2000 mm and a clear span of 1800 mm, were utilized in this study. Lap splicing was employed in the tested beams to establish a controlled weak region, thereby simulating a localized incident. Consequently, using a splice length shorter than the recommended ACI value prevents reinforcement from yielding in flexure, failing by debonding or bond-slip at the splice. The reference beam specimen had no mid-span splice, so the reinforcement was continuous. The other reinforced concrete beams were lap-spliced at their centers. Three 12 mm deformed steel bars served as the primary longitudinal reinforcement. The beam splice specimen design utilized 70% of the predicted development length, based on earlier work by [22]. The adopted splice length was 200 mm, and lap splicing was used, which is below the recommended value in the ACI Code; as a result, the specimens are likely to experience debonding of the lap-spliced bars. Stirrup spacing was reduced to ensure that a shear failure would not occur before a bond failure. The stirrups were not placed within the lap spliced area to avoid being confined inside the splice zone. Within the stirrups, two bars, each 10 mm in diameter, located in the top part of the section, served as the primary reinforcement in the compression zone to align and stabilize the reinforcement cage. According to the ACI Code, the concrete cover was specified to be 25 mm, which is the recommended minimum concrete cover to ensure a complete bond between the steel bars and the concrete. Fig. 1 illustrates the details of the reinforcement used in the tested specimens. The severe damage was intentionally inflicted by exerting a load equivalent to approximately 70% of the control beam's ultimate load, which is about 126 kN. The preloading procedure, as previously stated, may significantly diminish the load-bearing capacity of the tested specimens, given that it surpasses the service limit of the reference specimen when considering the lap-splice effect. The concrete cover has been scraped away, which is 300 mm wide and reaches the height of the concrete cover, leaving the steel bars uncovered to simulate damage in the lower area of the concrete beams, as illustrated in Fig. 2.

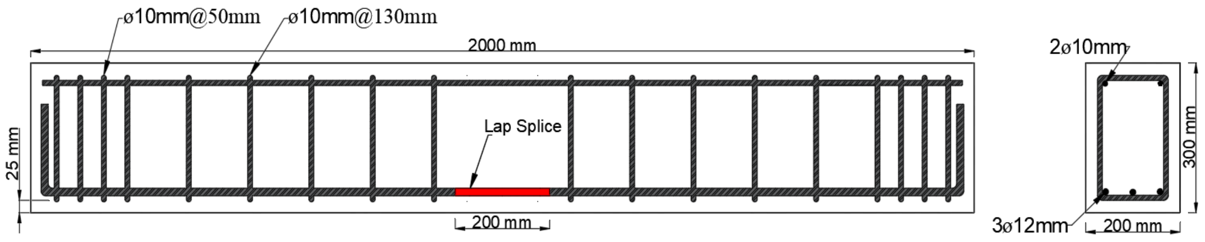

Fig. 1. Details of reinforcement: (a) front view, (b) cross-section.

Fig. 2. Damage at the bottom of the specimens (Inverted Specimens).

The matrix of the work followed a methodology that involved studying four parameters. The first parameter examined the effect of the shape of repairing bars, comparing the performance of bars with hooked ends to that of straight ones. The second parameter evaluated the bond material, comparing the cementitious material used as a bond agent to the epoxy one. The third parameter involved in assessing the role of confinement by external repair through a steel plate attached with a bonding agent and fixed in the middle of the span by nails. The fourth and final parameter investigated the impact of the diameter of repairenening bars, comparing the performance of a larger diameter of 16 mm with a smaller one of 12 mm. Table. 1 outlines the details of the tested specimens, including the coding procedure.

Table 1. Specimen details.

Number	Specimen	Configuration of Strengthening Bars	Confinement by Steel Plate	Diameter of Strengthening Bars (mm)	Bonding Material
1	BC*	N.A.**	N.A.	N.A.	N.A.
2	HCE12	Hook	with	12	Epoxy
3	SCE12	Straight	with	12	Epoxy
4	HCM12	Hook	without	12	CM***
5	HE12	Hook	without	12	Epoxy
6	HCM16	Hook	without	16	CM
7	HE16	Hook	without	16	Epoxy
8	HCCM12	Hook	with	12	CM

*BC= Control Beam, **N.A. = Not Applied, **CM = Cementitious material.

4.2. Repairing procedure

The beams were installed upside down, with the soffit at the top, to facilitate more straightforward repairs in the lab. Under and around the reinforcements, damaged and broken concrete was scraped away utilizing a pneumatic hammer. The rebar was cleaned with a wire brush, allowing a better bond with the new repair materials.

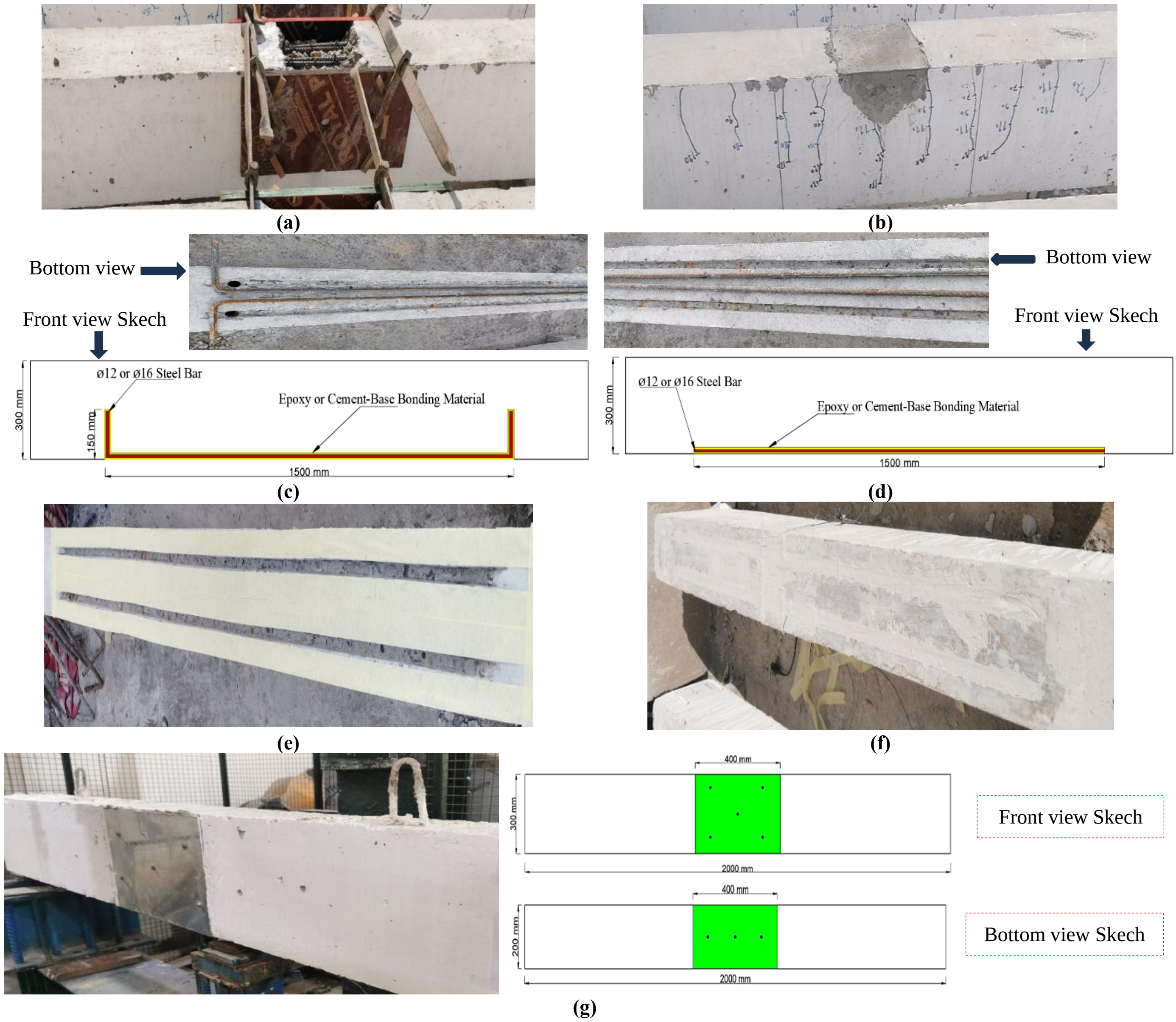

Fig. 3. Repairing procedure; (a) preparing to pour SCC layer, (b) after pouring and leveling the surfaces of SCC layer, (c) hooked ends repairing bars, (d) straight state repairing bars, (e) drilling grooves, (f) filling grooves with bonding agent, (g) repairing with an externally bonded steel plate.

Additionally, employing a high-pressure air jet, dust and loose particles were expelled from the surface. The surface was moistened with water before the mending concrete was put in. The damaged concrete was repaired through self-compacting concrete (SCC), which is characterized by high deformability and the ability to flow through spaces between steel reinforcing bars without segregation or blocking, as demonstrated in Fig. 3, a and b.

All repaired specimens were repaired with two steel bars, each 1500 mm long and 10 mm in diameter. The specimens with hooked repair bars were bent at both ends so that the free vertical ends extended 150 mm. This hook was designed in accordance with ACI 318-19 [23], which requires a 90-degree bend with a minimum bend diameter of 75 mm, as illustrated in Fig. 3, c and d.

The repair process using the NSM approach was started by carving grooves into the concrete cover at the bottom of all specimens, except the control. These grooves were drilled approximately 1.5 to 2 times the diameter of the steel bar-NSM, depending on the bonding material. Grooves were made with a concrete cutter, and any leftover concrete lumps were removed. The bottom surface of the grooves was roughened with a hammer and a hand chisel. Based on the paper methodology, two adhesive materials were used: epoxy and cementitious material, depending on the specimen type tested. These materials functioned as the bonding agents for attaching the steel rebar to the concrete. Fig. 3, e and f, reveals the NSM technique procedures.

In specimens with a steel plate, the plate covered both sides and the bottom part of the beam section, extending horizontally for 400 mm, centered at the middle portion of the beam, as shown in Fig. 3, g. The steel plate was fixed in place with epoxy and nets.

4.3. Mix properties

All of the concrete components in the test program were cast using either regular or self-compacting concrete. The NCM utilized 440 kg/m³ of cement and a water-to-cement (W/C) ratio of 0.4. The aggregate proportions included 690 kg/m³ of fine aggregate and 1000 kg/m³ of coarse aggregate. In the SCC mixture, 368 kg/m³ of cement was incorporated, and the W/C ratio was 0.45. The aggregate composition consisted of 754 kg/m³ of fine aggregate and 858 kg/m³ of coarse aggregate. Additionally, 10% silica fume (by weight of cement) was included to enhance its filling ability. The mix designs were based on mixes tested at 28 days, as specified in ACI 211-91 [24].

4.4. Materials properties

Ordinary Portland cement was used in casting all the specimens with sompressive strethegth of 29 MPa. The fine aggregate was sieved to 4.75 mm to remove particles larger than this size. Sand was used in a saturated state with a dry surface. The local gravel also had a maximum size of 19 mm. In this study, three deformable bars with diameters of 10mm, 12mm, and 16mm were used. The steel bars' mechanical test data show: the Ø10 mm bar had a yield stress of 526 MPa, ultimate stress of 730 MPa, and 10.2% elongation; the Ø12 mm bar had a yield stress of 550 MPa, ultimate stress of 751 MPa, and 12% elongation; the Ø16 mm bar had a yield stress of 540 MPa, ultimate stress of 710 MPa, and 12.3% elongation. These results are in accordance with ASTM A615M-24 [25] standards. The 2 mm steel plate was used for confinement. The ASTM A370-17 [26] guidelines were followed to create coupon samples. The steel plate had a yield stress of 274 MPa, an ultimate stress of 454 MPa, and 20.8% elongation, which is below the 22% limit specified in ASTM A36/A36M-19 [27].

Two different adhesive materials were used: epoxy and cement-based adhesive. The epoxy adhesive employed in this study (Sikadur®-31 CF Normal) demonstrated superior mechanical strength and bonding efficacy, with a tensile strength of 21 MPa and tensile adhesion to concrete surpassing 4 MPa. Conversely, the cementitious adhesive (Keraflex Extra S1) exhibited an initial tensile adhesion strength of 2.3 MPa. It was classified as an S1 deformable adhesive characterized by an extended open time and excellent substrate compatibility. The mechanical characteristics of concrete were assessed, including compressive, tensile, and flexural strengths. The compressive strength of the concrete was measured on the 28th day of testing in accordance with ASTM C39/C39M-24 [28]. The tensile strength of concrete was evaluated using ASTM C496/C496M-17 [29] by analyzing the split tensile strength of three cylinders, each measuring 200 mm in length and 100 mm in diameter, during the beam testing period. The flexural strength test was performed on three prisms measuring 100 mm × 100 mm × 400 mm, in accordance with ASTM C78/C78M-22 [30]. Normal concrete exhibited a compressive strength of 28.2 MPa, a tensile strength of 3.02 MPa, and a flexural strength of 4.4 MPa. Conversely, SCC demonstrated strengths of 28.2 MPa, 2.35 MPa, and 3.88 MPa, respectively.

Regarding SCC, a slump flow test on fresh specimens to determine the workability of SCC was conducted. The slump flow test for fresh SCC resulted in a value of 677 mm, which complies with the EFNARC recommended limit of 650 to 800 mm [31].

4.5. Test setup

All beams were tested, as shown in Fig. 4. The specimens were cured for 28 days and then painted with white pigment to facilitate crack detection during loading. The tested beams were simply supported, with steel plates and rollers positioned over the supports and beneath the loading points to prevent local concrete crushing. The supports were placed 100 mm from each beam end, resulting in a clear span of 1800 mm. All specimens were tested under four-point bending. The load was applied vertically in incremental steps, and the corresponding deflection was recorded at each 5 kN load step. A linear variable displacement transducer (LVDT) was installed at the beam mid-span beneath the soffit to measure vertical deflection throughout the test. Crack initiation and propagation were visually monitored on painted beam surfaces, marked with a pencil/marker. Fine crack widths up to 0.5 mm were measured using a crack meter, while larger crack widths were measured using a digital vernier caliper. After repairing and during loading until failure, the cracks were highlighted with a marker pen. During testing, the maximum load capacity, deflection, and failure mode were documented.

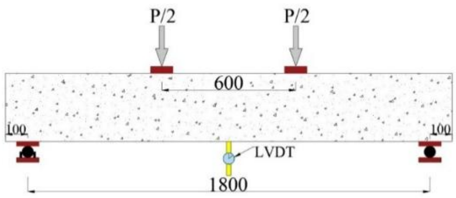

Fig. 4. Schematic details for application load and supports.

5. Experimental results

The load and corresponding deflection were recorded during all loading steps, and the load was incrementally increased up to failure. The first flexural crack was visually observed, and the corresponding load was identified. Table. 2 illustrates the test data regarding load and deflection for every tested beam specimen.

Table 2. Results of the test specimens for recorded data.

Specimens	Pcr (kN)	Δcr (mm)	Pu (kN)	Difference	Δu (mm)	Pu/Puc*
BC	25.2	0.59	180	---	19.35	1
HCE12	50	0.86	189	5.4%	6.11	1.1
SCE12	54	0.55	170	5.4%	8.12	0.9
HCM12	30	0.53	120	33.2%	4	0.7
HE12	35	0.63	148	17.6%	5.29	0.8
HCM16	30	0.36	163	9.3%	6.04	0.9
HE16	35	0.39	208	15.6%	8.1	1.2
HCCM12	40	0.74	199	10.6%	7.2	1.1

*Puc: Ultimate load of refernce specimen.

Ductility refers to the capacity of a structural element to maintain its load-bearing ability even after undergoing significant deformation or deflection. The ductility ratio (μ) is commonly defined as the ratio of the ultimate displacement to the displacement at yield, typically based on an idealized elastic–plastic response. The present study adopted an approach to calculate the yield displacement using the deflection corresponding to 75% of the ultimate load ($\Delta_{0.75}$Pu) proposed by Park [32]. For the tested repaired concrete beam specimens, the experimental ductility ratio (μ) was calculated by dividing the ultimate deflection (Δu) by the deflection at 75% of the peak load ($\Delta_{0.75}$Pu). Tab.3 presents the calculated ductility values for all tested specimens.

Two types of stiffness values were adopted in this study: initial stiffness and service stiffness. The initial stiffness was defined as the slope of the load–deflection response in the pre-cracking stage, i.e., before the appearance of the first visible crack [33]. It is common to estimate initial stiffness using the cracking load or a value below it. The analysis revealed that the lowest recorded cracking load corresponded to approximately 14% of the ultimate load. To ensure consistency and to remain safely within the elastic range, 10% of the ultimate load (Pu) was selected as the standard reference point for evaluating the initial stiffness. The service stiffness was determined based on the structural response under service-level loading, typically where deflection limits and cracking control are of primary concern. In this context, the service stiffness was calculated using a serviceability-based approach, corresponding to 65% of the ultimate load (0.65 Pu) [34, 35]. The computed values of both initial and service stiffness for all tested specimens are outlined in Table.3.

Table 3. Results of the test specimens for calculated data.

Specimen	Initial stiffness (kN/mm)	Service Stiffness (kN/mm)	Ductility Index (μ)	μ/μ_c*	Energy Absorption (kN.m) (EA)	EA/EA_c**
BC	44.2	27.1	3.84	1	4.451	1
HCE12	57.1	47.8	1.93	0.503	1.355	0.304
SCE12	100.0	89.1	5.62	1.464	1.519	0.341
HCM12	54.5	41.9	1.72	0.448	0.478	0.107
HE12	64.4	39.1	1.71	0.445	0.936	0.210
HCM16	79.7	25.5	3.2	0.833	1.009	0.227
HE16	109.3	20.8	3	0.781	1.819	0.409
HCCM12	85.1	39.7	1.75	0.456	1.488	0.334

*μc: Ductility of refernce specimen, *EAc: Energy absorption of refernce specimen.

The energy absorption capacity of reinforced concrete beam specimens is determined by calculating the area under the load-deflection curve, which represents the total energy absorbed by the specimen from the initiation of loading up to the point of failure. This area encompasses the entire deformation process of the beam, capturing both elastic and inelastic behavior, and provides insight into the beam's ability to undergo considerable displacements while maintaining structural integrity [36]. The present study calculated the energy absorption capacities of all tested specimens. This enables a consistent and comparative assessment of how different repairing configurations affect the energy dissipation behavior of the beams. Tab.3 reports the resulting values for each specimen.

6. Parameters

6.1. Effect of hooked bar

Two configurations for repairing steel bars, straight and hooked steel bars, were used to evaluate the impact of the hooked bar pattern on the effectiveness of the repair. One group of specimens was employed for this purpose: SCE12 and HCE12. Fig.5 illustrates the load mid-span deflection curves for specimens related to the current investigated parameter.

At the first cracking stage, the load values were 54 and 50 kN, respectively, resulting in increases of 113.9% and 98.8% for SCE12 and HCE12, respectively, compared to the reference specimen BC. The deflection at the cracking stage demonstrated two behaviors. For specimens with a hooked repairening bar, deflection increased by up to 45.9% corresponding to the HCE12 specimen, more than in the reference specimen BC. In contrast, the specimens with straight repairening bars, SCE12, exhibited a slight drop in deflection of 6.6%.

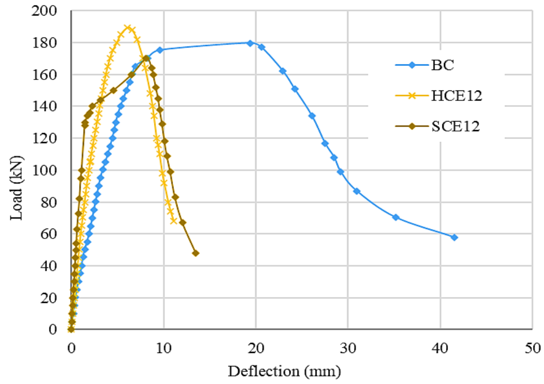

Fig. 5. Load to mid-span curves for specimens with hooked and straight ends.

At the ultimate loading stage, the hooked repairening pattern in the HCE12 specimen demonstrated an improved load-carrying capacity of 189, exceeding that found in the reference specimen BC by approximately 5%. Additionally, the load capacity in the straight repairening bars of the SCE12 specimen reached 170, representing a recovered capacity of roughly 94.5%, compared to the reference specimen BC. The ultimate deflection at failure significantly drops for all specimens tested and is correlated to the current study parameter. The recorded ultimate deflections were 8.12 and 6.11 mm, reflecting decreases of approximately 58% and 68.4% corresponding to specimens with straight and hooked ends, respectively, relative to the reference specimen BC.

Regarding the stiffness values, all repaired specimens exhibited a considerable increase in stiffness, either at the initial or service state, with the most notable improvement occurring at the service stiffness and for specimens with a straight repair bar. The specimen with hooked repairing steel bars exhibited a 29.2% enhancement in initial stiffness. Regarding service stiffness, it was 76.2%, which is higher than that of the reference specimen BC. The initial stiffness of the SCE12 specimen using straight repairening steel bars was enhanced by 126.4%, while the service stiffness of this specimen improved by 228.4% over the BC specimen. Fig. 6 demonstrates the effect of repairing the steel bar configuration on both initial and service stiffness.

The ductility values were positively affected in a specimen repaired by straight steel bars, where specimen SCE12 exhibited an increase in ductility by about 46.4%, relative to the reference specimen BC. In contrast, the HCE12 specimen with a hook-repairing steel bar suffered from a reduction in ductility by approximately 49.7% relative to the reference specimen BC. The energy absorption for the entire set of tested specimens, regarding the examined parameter, decreased by approximately 65.9% and 69.6% for SCE12 and HCE12 specimens, respectively, in the same beam order, compared to the reference specimen BC. Fig. 7 demonstrates the effect of repairing the steel bar configuration on ductility and energy absorption for each specimen tested under the current study parameters.

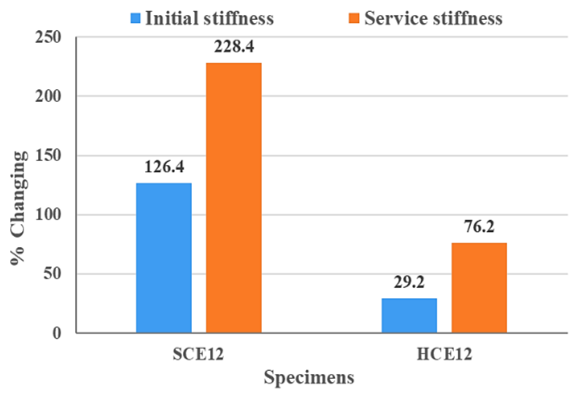

Fig. 6. The effect of repairing steel bar configuration on initial and service stiffnesses.

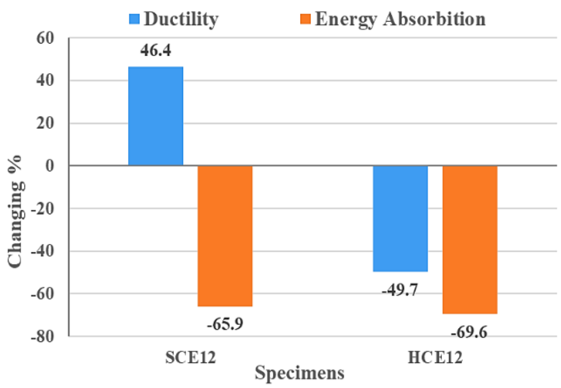

Fig.7. The effect of repairening steel bar configuration on ductility and energy absorption.

NSM steel bar repair systems were implemented on all repair specimens, resulting in a delayed onset of cracking compared to the unrepaired control beam. Hook-end-bar reinforcement demonstrated a more ductile response during cracking, which can be attributed to the enhanced mechanical anchorage and bond between the reinforcement and the concrete. However, this configuration also introduced localized stress concentrations near the hook areas, resulting in earlier crack formation under higher loads and a subsequent decrease in overall ductility. Straight steel bars, on the other hand, exhibited a stiffer response at the start of cracking but maintained better ductility and service stiffness because of uniform stress distribution and continuous alignment, which allowed for efficient load transfer. Although hooked bar specimens exhibited an increased ultimate load-carrying capacity, both repairing strategies reduced deflection at failure and decreased energy absorption, illustrating the typical trade-off between increased strength and reduced deformation after yield. While hooked bars provided better anchorage and peak strength, straight bars provided better stiffness characteristics during service loading conditions.The straight-bar setup likely ensured a more uniform bond stress and direct load transfer along the NSM groove, increasing stiffness and reducing early deformation. Conversely, the hooked-end anchorage of specimen HCE12 may have caused localized stress, microcracking, and uneven strain near the bends, thereby lowering stiffness.

6.2. Effect of adhesive material

This part of the study evaluated the effect of the bond material. Two groups of specimens were used: the first involved specimens HE12 and HCM12, and the second involved HCCM12 and HCE12 specimens. Fig. 8 demonstrates the curves of load-mid span deflection for specimens relevant to the present study's parameters. All repairing approaches using epoxy or cementitious material as a bonding substance showed a higher load at first cracking than the reference BC specimen. The specimens that used epoxy as an adhesive material had the most prominent enhancement. The HE12 and HCE12 (used epoxy) recorded the first crack at a load of 35 and 50 kN, with an increase of 39.4% and 98.8%, respectively, over the reference beam specimen BC. The HCM12 and HCCM12 specimens with cementitious material as an adhesive developed an initial crack at a load of 30 and 40 kN, with a gain of 18.8% and 59.3%, respectively, which is greater than that of the reference beam specimen BC. The specimen that used epoxy revealed an increase in cracking deflection of approximately 7.6% and 45.9%, while the specimens utilizing cementitious material showed a 10.7% drop in HCM12 or an increase in HCCM12 by 26.1%.

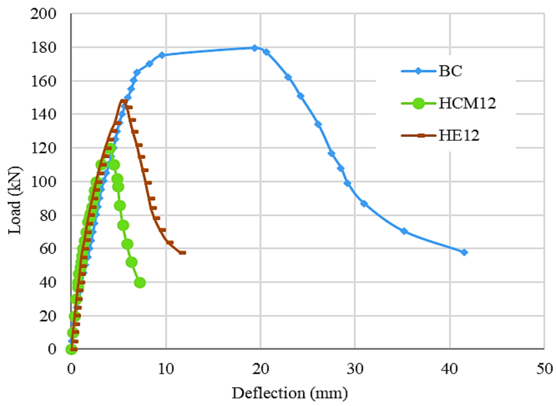

(a)

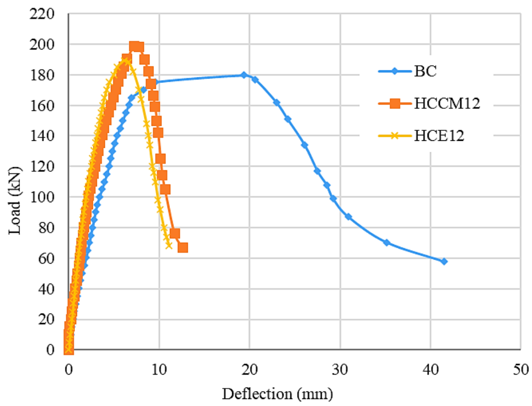

(b)

Fig. 8. Load to mid-span curves for specimens with epoxy and cementitious bond agents; (a) group 1 specimens, (b) group 2 specimens.

The repair with epoxy (in the HE12 specimen), in group 1, restored 83.4% of the bearing capacity of the BC reference specimen, outperforming the repair with cementitious material (in the HCM12 specimen), which restored 66.8%. In group 2, the repair using epoxy in the HCE12 exceeded the load capacity of the BC by only 5.6%, and in the HCCM12, the repair using cementitious material exceeded it by 10.6%. There was a clear trend toward reduced ultimate deflection in all specimens repaired with any bonding material. Specimens repaired with epoxy and a cementitious material experienced reductions in ultimate deflection of 72.7% and 79.3%, respectively. A noticeable contrast in stiffness performance was noted between specimens bonded with epoxy and those bonded with cementitious material. Epoxy-repaired specimens generally demonstrated more uniform improvement in initial and service stiffness values, with moderate improvements observed in HE12 by 45.8% and 44.2%, respectively. In contrast, HCM12 exhibited uneven behavior, indicating that it had improved service in stiffness, reaching 54.5% compared to the initial value of only 23.5%. Moderate improvements were observed in HCE12, with 29.2% for initial stiffness and 76.2% for service stiffness, reflecting the positive effect of epoxy reining. In contrast, HCCM12 has inconsistent behavior, showing a reverse pattern with an initial stiffness increase of 92.6% and a service stiffness of only 46.4%. Fig. 9 illustrates the effect of the adhesive material on initial and service stiffnesses.

In general, all repaired specimens exhibited reductions in ductility and energy absorption compared to the control specimen. For ductility, the epoxy-bonded specimens showed a reduction between 49.7% and 55.6%, while the cementitious-bonded specimens decreased between 55.1% and 54.3%, relative to the reference specimen BC. The findings indicate that ductility was affected to a similar extent by using both adhesive materials, resulting in a decrease in ductility. For energy absorption, the specimen bonded with epoxy experienced reductions ranging from 69.6% to 79%, whereas that bonded with cementitious material experienced reductions from 66.6% to 89.3%, relative to the reference specimen BC. According to the findings, both approaches utilizing adhesive materials showed only a slight difference in the decline in maximum energy absorption levels. Fig. 10 demonstrates the influence of bond material on ductility and energy absorption for each tested specimen under the current study's parameters.

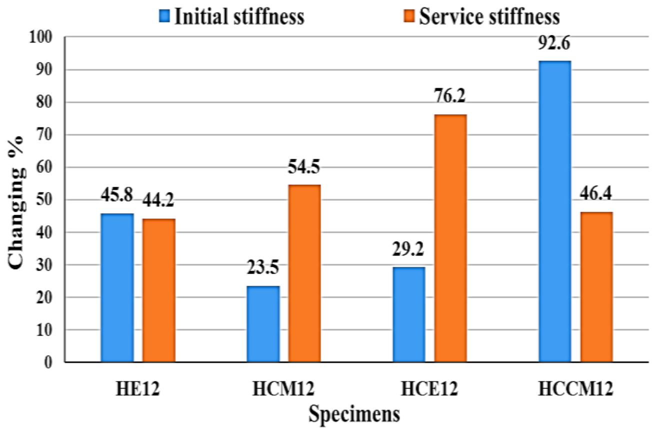

Fig. 9. The effect of bond material on initial and service stiffnesses.

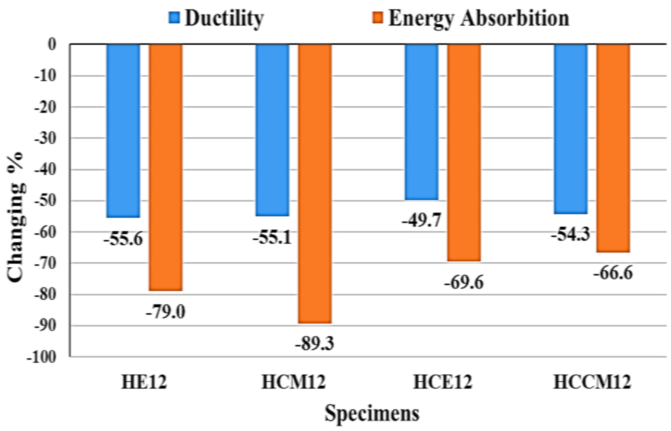

Fig. 10. The effect of bond material on ductility and energy absorption.

The improved cracking resistance seen in the repaired specimen is mainly due to the adhesive bonding layer, which helped effectively transfer stress between the concrete substrate and the embedded steel reinforcement. In comparison to the cementitious-bonded counterpart, the epoxy-bonded specimens consistently achieved higher cracking loads and greater initial stiffness, owing to their superior mechanical properties and bond efficiency at the adhesive interface. At the ultimate load stage, the epoxy-bonded beam demonstrated higher load-carrying capacity and improved anchorage performance, while the cementitious material showed lesser strength gains. Regarding deformation behavior, the cementitious-bonded beam exhibited a more significant reduction in ductility and ultimate deflection compared to the control specimen. Specimens bonded with epoxy also showed more consistent improvements in both initial and service-stage stiffness, and also maintained more post-peak energy capacity.

6.3. Effect of confinement

The confinement effect using a steel plate was evaluated with two specimens, HE12 and HCE12. Fig.11 shows the curves of load-mid span deflection for specimens associated with the current investigated parameter. Generally, all repairing methods, whether with or without confinement, noticeably delayed the initial flexural crack; however, confinement had a significant impact compared to a reference specimen. The specimen with confinement HCE12 recorded a first cracking load equal to 50 kN with an increase of approximately 98.8% over the control specimens BC. The specimens free of confinement HE12 had a cracking load of as much as

35 kN, with an improvement relative to the reference specimen BC of up to 38.6%. The deflection in a confined specimen rose to 45.9% against the reference specimen BC. In contrast, the unconfined specimens either revealed a modest increase in cracking deflection by 7.6%.

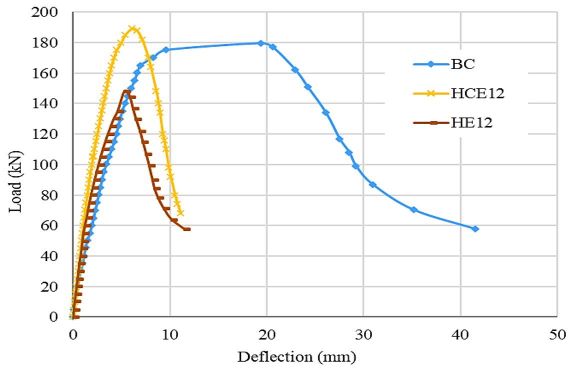

Fig. 11. Load to mid-span curves for specimens with and without confinements.

The confinement was also effective in a more pronounced manner at the ultimate stage. In the ultimate stage of loading, the load capacity was greater than that of the reference specimen BC, with 5.4% in the confined specimen. In contrast, the corresponding unconfined specimen HE12 restored only 82.4% of the original capacity of the reference specimen. The effect of steel plate confinement on ultimate deflection was assessed, where the non-confined specimen HE12 showed a 72.7% reduction in ultimate deflection. Conversely, the confined specimen HCE12 experienced a slightly lower reduction of 68.4%.

Confinement led to a gain in initial and service stiffnesses. The outcomes revealed that the improvement in initial and service stiffnesses was nearly the same in specimens lacking confinement. Conversely, the presence of confinement increased service stiffness more than the initial stiffness. The specimen with confinement HCE12 improved initial stiffness by around 29.2%. In contrast, the specimen free of confinement HE12 enhanced initial stiffness by around 45.8%, for the same specimen order, compared to the reference BC specimen. For stiffness values at the service stage, the unconfined specimen HE12 experiences a boost of 44.2% versus the BC reference specimen, with a semi-identical grade to the initial stiffness. The specimen with confinement exhibited substantial gains in service stiffness, as much as 76.2% against the BC reference specimen BC, and larger than the initial stiffness values. Fig.12 demonstrates the influence of confinement on initial and service stiffnesses.

The specimens that were repaired, either with or without confinement, generally experienced a reduction in ductility compared to the reference BC specimen. The specimens HE12 and HCE12 (unconfined and confined, respectively) exhibited ductility decreases of approximately 55.6% and 49.7% respectively. All tested specimens, regardless of confinement, also suffered from a reduction in energy absorption. The HE12 and HCE12 showed significant decreases of 79% and 69.6%, respectively. Fig.13 reveals the influence of confinement on ductility and energy absorption for every tested specimen under the present investigated parameters.

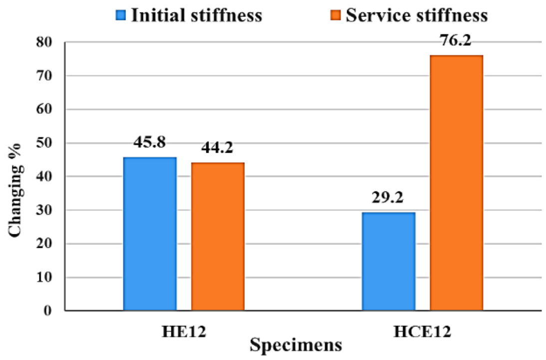

Fig. 12. The effect of confinement on initial and service stiffnesses.

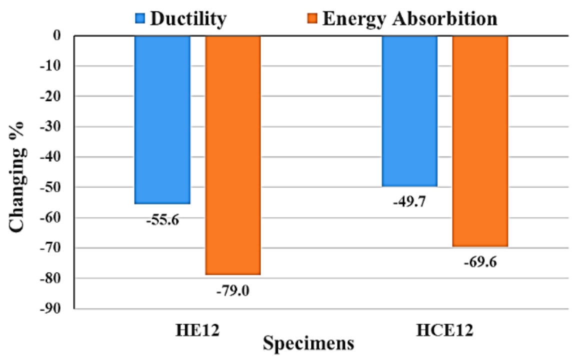

Fig. 13. The effect of confinement on ductility and energy absorption.

The improved structural behavior seen in confined reinforced concrete beams mainly results from the lateral restraint offered by externally attached steel plates, which effectively reduces transverse deformation in the tension zone and delays the start and spread of both splitting and flexural cracks. This confinement not only enhances the tensile strength of the concrete section but also permits greater deflection before cracking. Additionally, during final loading stages, the confinement significantly boosts the ultimate load capacity by improving the mechanical anchorage of repairing bars, preventing bar-concrete separation, and delaying crack propagation. Comparative experimental results show that confined specimens experienced smaller decreases in deflection compared to their unconfined counterparts, emphasizing the importance of confinement in enhancing deformation capacity and load resistance.

Although unconfined beams initially display higher stiffness because of stronger early NSM bonding, confined specimens exhibit greater service stiffness after cracking due to better crack control. However, a general decrease in ductility is observed across all repaired systems, mainly because increased stiffness and early crack suppression restrict plastic deformation and curvature capacity. While confinement does not directly improve ductility, it reduces its decline. The efficiency of the steel plate confinement system is further enhanced by mechanical nets, which keep the plate and concrete in strong contact, prevent early debonding, and ensure force transfer across the interface.

6.4. Effect of repair bar diameter

In this part of the results discussion, the influence of the diameter of the repairening bar was assessed. The specimens were organized into pairs, with one specimen having 12mm repair bars and the other measuring 16mm in diameter. The specimen groups were: Group 1 (HE12 and HE16) and Group 2 (HCE12 and HCE16). Fig.14 illustrates the curves of load-mid span deflection for specimens related to the currently studied parameter. For the HE specimens (group 1), the cracking load increased notably compared with BC. Both HE12 and HE16 carried 35 kN, corresponding to a 40% improvement over the control. However, cracking deflection showed different behavior: HE12 exhibited a slight increase of 7.6%, while HE16 experienced a reduction of 33.8% compared with BC. This indicates that the bar diameter did not affect the initial cracking load, but it reduced the deflection considerably. For the HCM specimens (group 2), the cracking load improved by 20% compared with BC, with both HCM12 and HCM16 reaching 30 kN. However, cracking deflection decreased in both cases: HCM12 was 10.7% lower, and HCM16 experienced a more severe reduction of 38.9% compared with BC. This reflects the almost identical trend of behavior as in group 1.

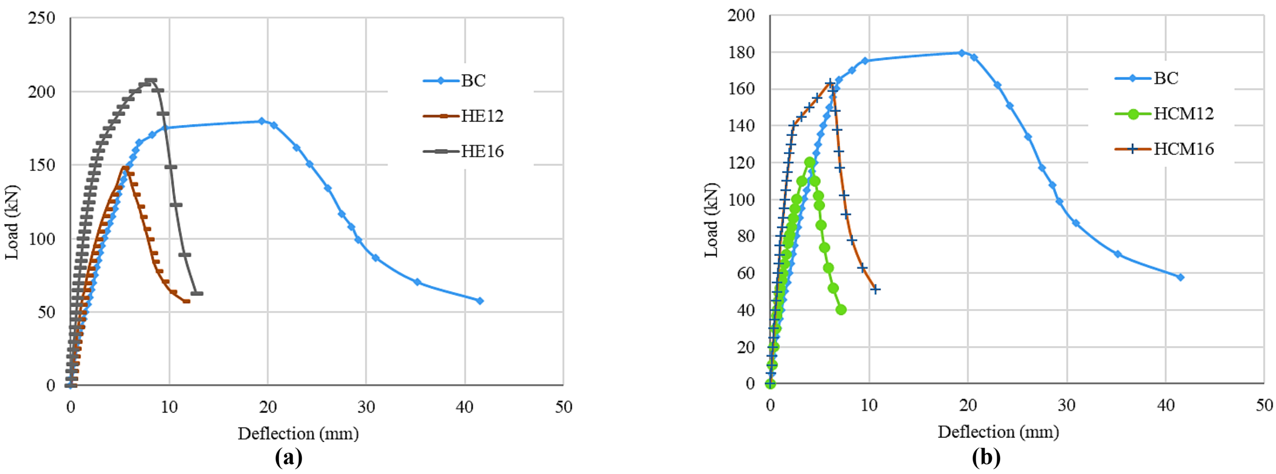

Fig. 14. Load to deflection curves for specimens with repairing bars of 12 mm and 16 mm; (a) group 1 specimens, (b) group 2 specimens.

The influence of steel bar diameter on the ultimate load capacity demonstrated apparent variation across the tested specimen groups relative to the value in the reference BC specimen. In the first group, the repair using steel bars of 12 mm diameter (HE12 specimen) restored 82.4% of the original capacity. In contrast, the specimen (HE16) with 16 mm diameter repairing bars exceeded the original capacity by 15.6% more than the BC reference specimen. The outcomes of the second group of specimens referred to recovering 66.8% in a specimen (HCM12) with a 12mm repairening bar diameter and an even higher ratio in the specimen (HCM16) containing a 16 mm repairening steel bar, reaching 90.7%, compared to the BC reference specimen.

The influence of steel bar diameter on the ultimate deflection exhibited notable variation across the tested specimen groups relative to the reference BC specimen. In the first group, the specimen repaired with 12 mm bars (HE12) showed a 72.7% reduction in deflection, while the specimen with 16 mm bars (HE16) exhibited a smaller decrease of 58.1%. The second group reflected a similar trend, with the HCM12 specimen (12 mm diameter) showing the highest reduction of 79.3%, compared to 68.8% for the HCM16 specimen (16 mm diameter).

Initial and service stiffness, using repairing bars with a diameter of 12 mm or 16 mm, led to a considerable improvement in these stiffnesses. The distinct context for the stiffness values was evident in more substantial increases in service stiffness, higher than the initial one, in most beam specimens. These increases were greater in specimens with a 16mm diameter of the repairing steel bar than in those with a 12 mm bar. For specimens repaired with 12 mm steel bars, the initial stiffness increased from 23.5% to 45.8%, while service stiffness improvements ranged from 44.2% to 54.5%. In comparison, specimens repaired with 16 mm steel bars exhibited greater enhancement, with initial stiffness increasing between 84.5% and 147.5% and service stiffness ranging from 145.1% to 151.9%. These results confirm that all repaired specimens outperformed the control in stiffness performance and that using 16 mm bars generally resulted in higher gains, particularly in service stiffness. Fig.15 shows the impact of the diameter of the repairing steel bar on initial and service stiffnesses.

All specimens exhibited reductions in ductility relative to the control specimen. The drop in ductility in the specimens with a 12 mm repairing bar ranged between 55.1% to 55.6%, while those with 16 mm bars were between 16.8% to 21.8%. These results verify the positive effect on ductility from larger bar diameters. Although the increase in bar diameter did not enhance ductility, it contributed to reducing the extent of ductility loss in most specimens. The energy absorption performance showed less improvement compared to ductility across all specimens as the repairing bar increased from 12 mm to 16 mm. All specimens experienced reductions relative to the reference specimen, with 12 mm bar specimens exhibiting reductions ranging from 79% to 89.3%. Specimens repaired with 16 mm bars displayed a decrease of 59.1% to 77.3%, indicating a less severe energy absorption loss than their 12 mm counterparts. This trend suggests that increasing the bar diameter may help mitigate the extent of energy dissipation loss. However, the overall performance remained below that of the original control specimen in all cases. Fig.16 illustrates the effect of the diameter of the repairening bar on ductility and energy absorption.

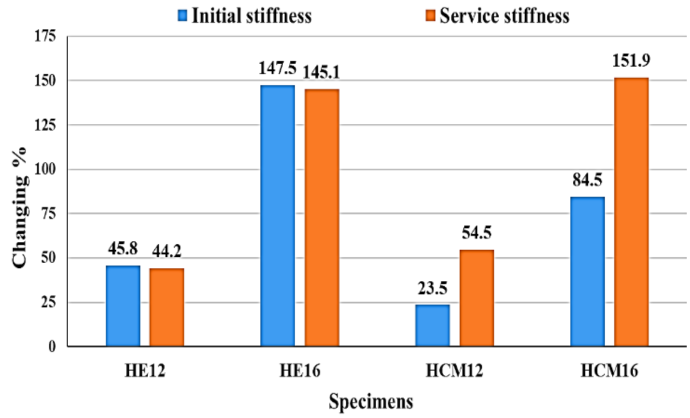

Fig. 15. The effect of repairing bar diameter on initial and service stiffnesses.

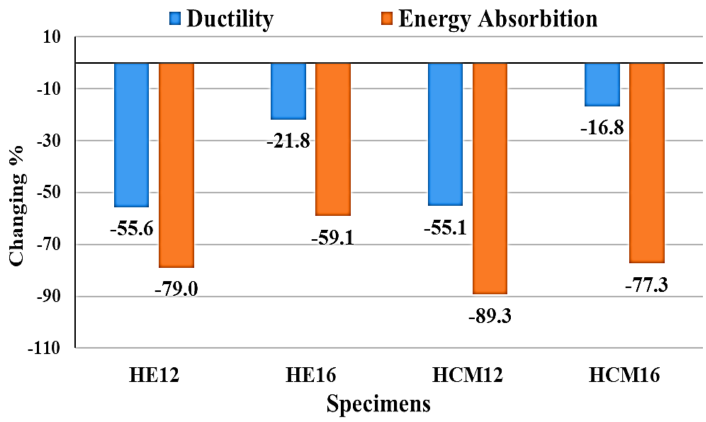

Fig. 16. The effect of repairing bar diameter on ductility and energy absorption.

Although stronger reinforcement bars theoretically provide better tensile resistance and control crack growth, experimental results show that these benefits do not always appear during early loading, when concrete's tensile strength mainly causes cracking, and reinforcement engagement is still limited. Since 16 mm bars have higher stiffness and less deformation capacity, they activate later and contribute minimally before cracking. Their structural effectiveness mainly appears in the post-cracking stage, when tensile stresses transfer from concrete to steel, enhancing stiffness, load capacity, and crack control during service. Compared to 16mm repairening bar diameter, 12 mm bars consistently result in greater reductions in first-cracking deflection. While 16mm bars maintain the stiffness in service, retain energy, and resist ultimate loads more effectively, they suffer from a loss of ductility. Unlike a control specimen, all repaired specimens showed reduced ductility and energy absorption, with 16 mm bars significantly mitigating these losses compared to 12 mm bars.

7. Response of load-deflection curves for repairing

A comparison of the load-deflection curves across all specimens reveals notable behavioral differences, influenced by the repairing materials, bar configuration, bonding material, and confinement. These can be summarized as follows:

7.1. Cracking behavior

All specimens exhibited an initial linear elastic response, with the slope of the initial segment reflecting initial stiffness. The control specimen BC demonstrated relatively high initial stiffness up to approximately 5 mm of deflection, with first cracking observed at approximately 25 kN. Conversely, epoxy-repaired specimens (HCE12, SCE12, HE12, HE16) exhibited delayed cracking, indicative of enhanced tensile resistance attributable to improved bond performance. Notably, SCE12 cracked at 54 kN, the highest among all specimens, primarily due to confinement effects and the robust adhesion provided by the epoxy resin. Cementitious-repaired specimens (HCM12, HCM16), on the other hand, cracked early, approximately 30 kN, despite having large-diameter bars in the HCM16 configuration. Confinement improves tensile cracking resistance even with a weaker bonding agent in HCCM12, as cracking began at about 40 kN. At first, the curve showed a steep slope, indicating good stiffness. Therefore, cementitious bonding alone does not provide adequate crack resistance, especially without confinement. The curve in HCCM12 begins with a linear ascending phase, indicating elastic behavior with effective initial stiffness. The first visible crack appeared at a load of about 40 kN, marking the onset of tensile cracking in the concrete. However, unlike the BC specimen, the transition from elastic to post-cracking behavior is gradual and not characterized by a sudden drop in stiffness.

7.2. Post-cracking and yielding behavior

The specimens entered a nonlinear phase after cracking. The control specimen sustained a near-linear response slightly beyond the cracking point. Epoxy-bonded specimens consistently exhibited higher yield loads and demonstrated a more stable post-cracking response. HCE12 and HE12 yielded at 142 kN and 111 kN, respectively, while HE16 yielded at the highest load of 156 kN, accompanied by a smooth curve and extended plastic deformation. These findings underscore the superior bond strength and energy dissipation capabilities inherent to epoxy-reinforced systems. SCE12 has a yield of 128 kN; however, what characterizes its behavior is the smooth curvature and the progressively reduced stiffness, which signify improved confinement effectiveness, even beyond the yield point. In contrast, cementitious systems (HCM12, HCM16) demonstrated lower yield loads of 90 kN and 122 kN, respectively, and experienced more abrupt transitions to failure. The HCCM12 specimen produced a relatively high load of approximately 149 kN, exceeding the performance of some epoxy-based configurations. However, in opposition to the epoxy-confined specimens, the post-yield curve of HCCM12 exhibited no curvature, indicating that although confinement postponed yielding, it was unable to eliminate stiffness control. In the HCM12 system, the interval between yield and failure was notably short, signifying limited ductility and a sudden decline in load-bearing capacity. In HCCM12As the load increased, the curve continued to rise in a steady, nonlinear manner. The yield load, defined according to Park's criterion, was approximately 149 kN. This yield point marks the end of the elastic regime and the beginning of significant inelastic deformation.

7.3. Post-yield performance and failure load

The BC specimen, despite its ductility, demonstrated a lower peak load of 175 kN and functioned as a benchmark for performance. The load plateau observed beyond yielding in BC underscores typical ductile behavior characterized by sustained energy absorption until failure. In contrast, HCM12 exhibited a flattened load-displacement curve beyond 100 kN and failed at approximately 120 kN, indicating limited energy absorption capacity and a brittle failure mode. Although HCM16 attained a peak load of 163 kN, its failure was characterized by the absence of a ductile plateau, thus reaffirming the somewhat limited post-yield behavior of cementitious materials. The specimen HCCM12subsequently reached its peak load of 199 kN, indicating a high load-bearing capacity but limited deformability. The absence of a distinct plateau or softening phase suggests a relatively brittle failure. Overall, specimen HCCM12 exhibited enhanced strength but compromised ductility and toughness, indicating a stiffness-governed failure mechanism. With an ultimate load of 199 kN, HCCM12 stands among the strongest specimens in terms of strength. Nevertheless, despite its robustness, the curve displayed no evident softening or ductile plateau before the peak load, indicating a failure characterized by stiffness-driven brittleness.

8. Failure mode

The first series of failures due to flexure cracking with compression crushing was observed in both control BC and epoxy-bonded HE12 specimens. HE12 exhibits a flexural mode similar to the control beam, manifesting a bond transfer effect due to epoxy and retaining part of its load capacity. A second series of failures involved a bond-related mechanism primarily characterized by cover separation and debonding of repairing bars, as demonstrated by SCE12 and HCM12. For SCE12, using straight bars, even when confined with epoxy-bonded steel plates, resulted in limited anchorage efficiency, causing premature cover separation and subsequent plate debonding. Similarly, HCM12, which utilized hooked bars adhered with a cementitious material, failed due to inadequate bond strength, resulting in the premature detachment of the concrete cover. In a third series, flexural-shear failures occurred in HCE12, HCCM12, and HCM16. In the confined specimen HCE12, hook bars and epoxy were used as bonding agents; however, shear cracking developed and caused debonding of the steel plate. Contrary to HCM16, which included larger-diameter bars without confinement, it failed in a similar flexural-shear manner due to elevated shear stresses, compounded by limited bonding capacity. In HCCM12 with hooked NSM bars and a confined steel plate, both repair methods caused the beam to develop additional stresses until shear cracks appeared, along with flexural failure; however, the steel plate debonded because the cementitious material can withstand less stress than epoxy under the same conditions. HE16 also demonstrated complex mixed-mode failures. With 16mm hooked bars bonded with epoxy, the specimen exhibited flexural cracking, concrete splitting, and compression crushing. Due to the larger bar diameter, bond-induced splitting stresses were effectively transferred to the surrounding concrete, eventually triggering splitting cracks. Overall, epoxy-bonded specimens suffered flexural or flexural-splitting failures. A cementitious-bonded specimen, on the other hand, was prone to premature cover separation. The effectiveness of steel plate confinement in delaying debonding-related failures is highly dependent on anchorage configuration. Larger diameter bars altered the governing failure mechanism by introducing additional splitting stresses, while hooked bars maintained bond integrity better than straight bars. Fig. 17 illustrates all failure patterns observed in the tested specimens.

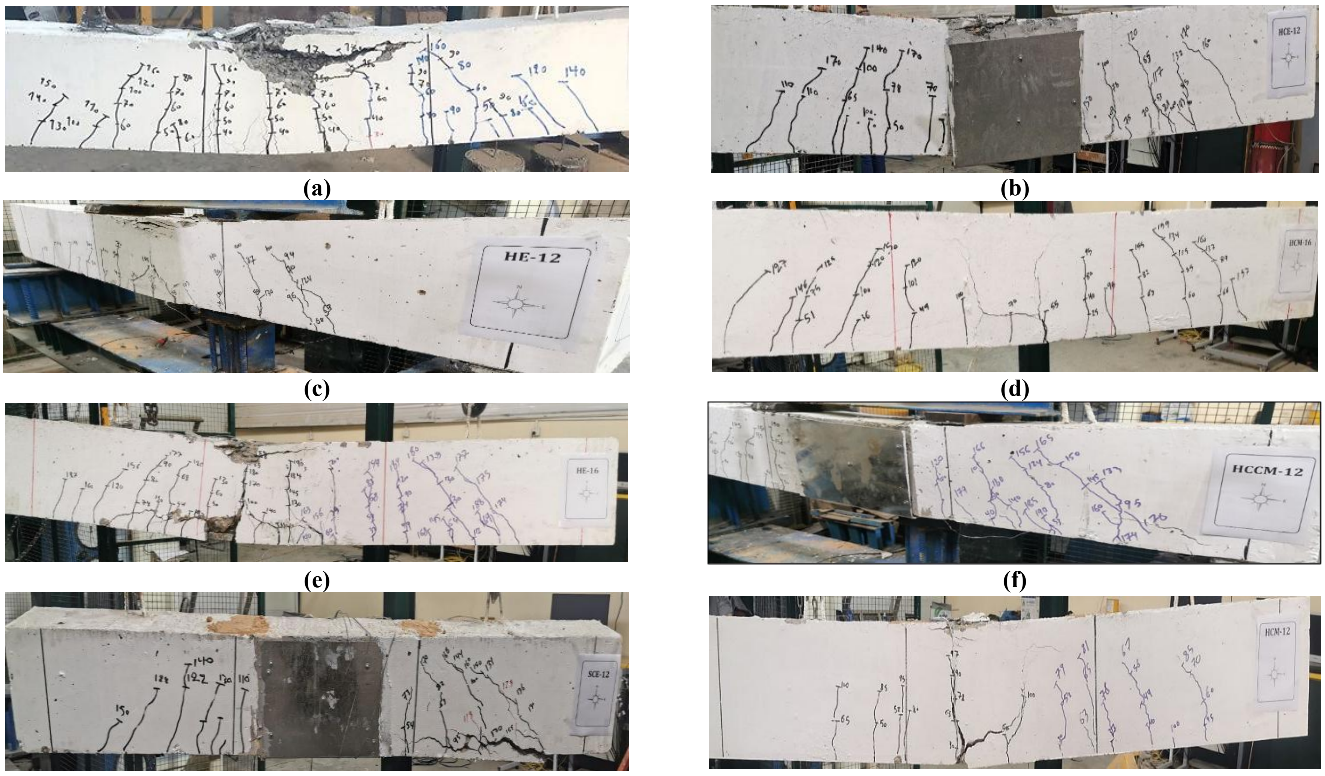

Fig. 17. Failure modes in specimens; (a) BC, (b) HCE12, (c) SCE12, (d) HCM12, (e) HE12, (f) HCM16, (g) HE16, (h) HCCM12.

9. Dimensionless comparison

The relative performance indicators presented in the Fig.18 provide a comprehensive assessment of the influence of the four investigated parameters on the flexural behavior of the repaired beams. Regarding bar-end configuration, the use of hooked-end bars increased the strength retention ratio from 0.945 for straight bars to 1.05, confirming the beneficial role of enhanced anchorage and improved bond mobilization. However, this increase in strength was accompanied by a substantial reduction in the ductility ratio, from 1.46 to 0.50, and a decrease in the energy dissipation ratio, from 0.342 to 0.304, indicating a stiffer response and a more brittle failure mechanism. Accordingly, straight bars provided a more even combination of strength, deformability, and toughness. The bonding material also exerted a pronounced influence on repair efficiency. For unconfined specimens, replacing cementitious adhesive with epoxy adhesive increased the strength retention ratio from 0.667 to 0.823, while the energy dissipation ratio improved from 0.108 to 0.210. These results reflect the superior bond characteristics, stress transfer efficiency, and composite interaction associated with epoxy systems. Under confined conditions, however, the differences between adhesive types became less significant, as the external confinement mechanism partially compensated for the weaker bond characteristics of the cementitious adhesive. The addition of external steel plate confinement consistently enhanced all principal response indices. The strength retention ratio increased from 0.823 to 1.05, the ductility ratio rose from 0.446 to 0.503, and the energy dissipation ratio improved from 0.210 to 0.304. This confirms that confinement effectively restrained crack propagation, stabilized the damaged mid-span region, delayed local deterioration, and improved post-yield response. Increasing the repair bar diameter from 12 mm to 16 mm produced one of the most favorable overall trends. For epoxy-bonded specimens, the strength retention ratio increased from 0.823 to 1.156, while the energy dissipation ratio rose from 0.210 to 0.409. For cementitious-bonded specimens, the corresponding values increased from 0.667 to 0.907 and from 0.108 to 0.227, respectively, with a concurrent improvement in ductility. Collectively, these findings indicate that increasing bar diameter and applying external confinement provided the most balanced enhancement in strength, ductility, and energy dissipation, whereas epoxy adhesive primarily improved bond-dependent behavior, and hooked-end bars mainly favored strength recovery at the expense of deformation capacity.

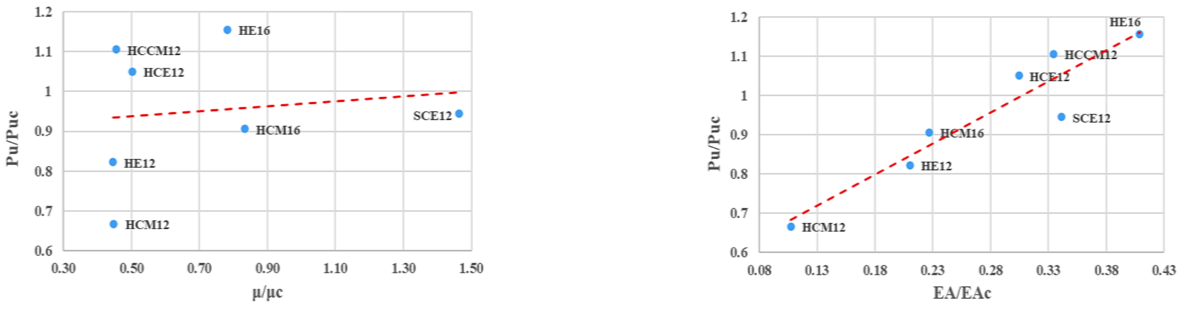

Fig. 18. Dimensionless comparison between load ratio (Pu/Puc) and: (a) ductility ratio (μ/μc), (b) energy dissipation ratio (EA/EAc).

10. Conclusions

The present study gives rise to several discernible conclusions, encapsulated succinctly in the following points:

1. The configuration of the repairing bars directly affected performance. At first, cracking, straight bars increased by 113.9%, while hooked bars grew by 98.1%. At ultimate load, hooked bars surpassed control by 5%, and straight bars recovered 94.5%. In stiffness, straight bars rose 126.4% in initial and 228.4% in service stiffness; hooked bars increased by 29.2% and 76.2%. Hooked bars may enhance anchorage at higher loads, but straight bars offer more efficient stiffness in elastic and serviceability ranges. Ductility improved by 46.4% with straight bars but decreased by 49.7% with hooked bars. Energy absorption declined 65.9% and 69.6%.
2. Hooked repair bars are a must, especially when anchorage deficiency, limited development length, or high debonding risk are present in conventional repair, particularly near damaged lap-splice zones or bar termination regions. However, they should be avoided for repairing beams found in seismic regions or areas exposed to cyclic loading, where high ductility, substantial post-yield deformation, and significant energy dissipation are essential. It is possible that straight-bar configurations will provide more balanced structural performance in these instances, or that hooked strengthening bars can be used in combination with another strengthening approach, such as confinement.
3. The bonding material also influenced repair outcomes. Epoxy increased the cracking load between 39.4% and 98.8%, whereas cementitious materials yielded smaller improvements from 18.8% to 59.3%. At the ultimate load, epoxy repairs restored between 83.4% and 105.6% of the control, while cementitious repairs ranged between 66.8% and 110.6%, depending on the confinement conditions. Stiffness values exhibited more consistent improvements with epoxy, showing increases of 29.2% to 45.8% in initial stiffness and 44.2% to 76.2% in service stiffness. Cementitious materials demonstrated less uniform results, with some cases achieving a 92.6% enhancement in initial stiffness but only 46.4% in service stiffness. Both adhesives significantly reduced ductility, with reductions from 49.7% to 55.6% for epoxy and from 54.3% to 55.1% for cementitious bonds. Additionally, energy absorption diminished from 66.6% to 89.3% across both bonding systems. Moreover, the utilization of hook-shaped strengthening bars, rather than conventional straight bars, effectively prevented debonding failure, a predominant and detrimental failure mode associated with the NSM strengthening technique.
4. Cement-based adhesives exhibit higher load-bearing capacity than undamaged reference specimens; however, they are less effective than epoxy-bonded systems. Their compatibility with concrete improves homogeneity and diminishes the likelihood of debonding or thermal stresses. Unlike epoxy, cementitious adhesive may be considered suitable for moderate-load or serviceability-governed structures, where economy, material availability, and ease of application are primary considerations. In contrast, epoxy adhesives are preferred for critical structural members and seismic-demanding applications, where considerable bond performance, higher energy dissipation, and more stable post-yield behavior are essential.
5. Beams repaired with 12 mm bars restored from 66.8% to 82.4% of their control ultimate capacity, while those repaired with 16 mm bars were restored to a range between 90.7% and 115.6%. Regarding ultimate deflection, a reduction between 72.7% and 79.3% was observed for beams repaired with 12 mm bars, whereas a decrease from 58.1% to 68.8% was noted for beams repaired with 16 mm bars. In the case of 12 mm bars, initial stiffness increased by 23.5 to 45.8%, whereas in the case of 16 mm bars, it increased by 84.5 to 147.5%. Service stiffness rose from 54.5% and 151.9% for 12- and 16-mm repairing bars, respectively, corresponding to the maximum gains. Ductility decreased by about 55% with 12 mm bars, but only in the range of 16.8 to 21.8% with 16 mm bars. Energy absorption losses were higher with smaller bars, ranging from 79% to 89.3%, compared to larger bars, which had losses from 59.1% to 77.3%.
6. The confined specimen demonstrated a remarkable increase in cracking load, which rose by 98.8% compared to a less dramatic increase of 38.6% observed in the unconfined case. At the ultimate load stage, the confinement resulted in a marginal yet significant enhancement of 5.4% over the control specimen. In contrast, the unconfined specimen managed to regain only 82.4% of its initial load capacity. In terms of initial stiffness, it was found that confinement contributed to a significant improvement of 29.2%. Meanwhile, the unconfined beams saw an even higher increase in stiffness, rising by 45.8%. However, in terms of service stiffness gains, confined beams outperformed their unconfined counterparts, achieving an impressive rise of 76.2% compared to just 44.2% for the unconfined beams. Ductility decreased in both confinement states in closer ratios. Furthermore, energy absorption capabilities were adversely affected, exhibiting a drop of 69.6% for confined specimens and an even more substantial 79% decline in non-confined specimens.
7. Epoxy-repaired beams showed flexural or flexural-splitting failures similar to the control. Cementitious specimens often failed by premature cover separation. Confinement produced flexural-shear failure with debonding of the steel plate, while larger bars tended to introduce splitting stresses in the concrete.
8. All specimens showed an initial linear-elastic response before cracking. Their later behavior depended on the repair medium and confinement. Epoxy systems performed better, delaying cracks, offering gradual post-cracking transitions, and improving ductility with stable energy dissipation, especially with confinement. Cementitious repairs often cracked early, had abrupt post-yield responses, and failed brittlely. Confinement helped, boosting strength and delaying cracks, but still resulted in stiffness-driven, brittle failure with higher ultimate strength.

9. The suggested NSM steel-bar repair system can restore load capacity, often exceeding the original strength. It reduces damage risk compared to external systems and allows localized repairs without demolition. It also enables the use of cheaper, locally available cementitious materials. However, for severely damaged RC beams requiring rapid restoration of flexural strength, stiffness, and serviceability under gravity and moderate loading conditions, the proposed repair method is not intended to be a seismic strengthening technique.

Based on the above results, it can be concluded that a suitable strengthening system, such as NSM, the use of hook-shaped steel repairing bars, can provide significant strength restoration even for severely damaged reinforced concrete beams, while also reducing or preventing debonding failure, which represents the common failure pattern of the NSM reinforcement system. Furthermore, the application of a bar binder, a component of the cementitious family, which is compatible in properties, is inexpensive and readily available, and yielded good results.

Statements & Declarations

Author contributions

Rasha A. Aljazaari: Investigation, Formal analysis, Resources, Writing - Original Draft, software, validation, and funding providing.

Javad Vaseghi Amiri: Conceptualization, Methodology, Project administration, Writing of Review and Editing, supervision.

Hayder Alghazali: Project administration, Writing of Review and Editing, and supervision.

All authors have read and agreed to the published version of the manuscript.

Acknowledgements

The author appreciates the Department of Civil Engineering, Noshirvani University of Technology, Babol, Iran, and the Engineering Consulting Bureau Laboratory, University of Kufa, for providing the necessary facilities for this research.

Funding

The authors received no financial support for the research, authorship, and/or publication of this article.

Declarations

The authors declare no conflict of interest.

Data availability

The data presented in this study are available on request from the corresponding author.

References

[1] Ivanova, I., Assih, J., Dontche, D. Repairing of short reinforced concrete corbel by bonding composite material under continuous load. In: 10th International Conference on Fracture Mechanics of Concrete and Concrete Structures; 2019; Porto (PT). p. 1–6. doi:10.21012/FC10.235590.

[2] Cerullo, D., Sennah, K., Azimi, H., Lam, C., Fam, A., Tharmabala, B. Experimental Study on Full-Scale Pretensioned Bridge Girder Damaged by Vehicle Impact and Repaired with Fiber-Reinforced Polymer Technology. Journal of Composites for Construction, 2013; 17: 662–672. doi:10.1061/(ASCE)CC.1943-5614.0000383.

[3] Al-Rifaie, W. N., Ismaeel, N. N., Riyad, H. Rehabilitation of Damaged Reinforced Concrete Beams. IOSR Journal of Mechanical and Civil Engineering 2017; 14: 58–70. doi:10.9790/1684-1403065870

[4] Nounu, G., Chaudhary, Z.-U. L. H. Reinforced concrete repairs in beams. Construction and Building Materials, 1999; 13: 195–212. doi:10.1016/S0950-0618(99)00014-8.

[5] Fayyadh, M. M., Abdul Razak, H. Assessment of effectiveness of CFRP repaired RC beams under different damage levels based on flexural stiffness. Construction and Building Materials, 2012; 37: 125–134. doi:10.1016/j.conbuildmat.2012.07.021.

[6] Haddad, R. H., Al-Mekhlafy, N., Ashteyat, A. M. Repair of heat-damaged reinforced concrete slabs using fibrous composite materials. Construction and Building Materials, 2011; 25: 1213–1221. doi:10.1016/j.conbuildmat.2010.09.033.

[7] Elkhatib, L., Khatib, J., Fırat, S., El Hassan, H., Elkordi, A. Rehabilitation of Concrete Structures - A Review. Gazi University Journal of Science, 2025; 38: 665–685. doi:10.35378/gujs.1503207.

[8] Alaee, F. J., Karihaloo, B. L. Retrofitting of Reinforced Concrete Beams with CARDIFRC. Journal of Composites for Construction, 2003; 7: 174–186. doi:10.1061/(ASCE)1090-0268(2003)7:3(174).

[9] Sevil Yaman, T. Behaviour of precast concrete beams prestressed with CFRP strands. Građevinar, 2016; 68: 775–786. doi:10.14256/JCE.1624.2016.

[10] Mashreia, M. A., Makkia, J. S., Sultana, A. A. Flexural Strengthening of Reinforced Concrete Beams Using Carbon Fiber Reinforced Polymer (CFRP) Sheets with Grooves. Latin American Journal of Solids and Structures, 2019; 16: e176. doi:10.1590/1679-78255514.

[11] Wu, H. C., Eamon, C. D. Strengthening of concrete structures using fiber reinforced polymers (FRP): design, construction and practical applications. 1st ed. Cambridge (UK): Woodhead Publishing; 2017.

[12] American Concrete Institute (ACI). ACI 440.2R-02: Guide for the design and construction of externally bonded FRP systems for strengthening concrete structures. Farmington Hills (MI): ACI; 2005. doi:10.1061/40753(171)159.

[13] Mostofinejad, D., Esfahani, M. R., Shomali, A. Experimental and numerical study of the RC beams shear-strengthened with NSM technique. Journal of Composite Materials, 2019; 53: 2377–2389. doi:10.1177/0021998319830777.

[14] Mirabi Banadaki, H., Eslami, A., Ronagh, H. Near-surface-mounted retrofitting of damaged/undamaged adobe walls using steel bars: Analytical evaluation of experimental results. Structures, 2020; 28: 2111–2121. doi:10.1016/j.istruc.2020.10.020.

[15] Rahman, M., Jumat, M., Hosen, M. A., Islam, A. B. M. Effect of adhesive replacement with cement mortar on NSM strengthened RC Beam. Revista de la construcción, 2016; 15: 61–72. doi:10.4067/S0718-915X2016000100006.

[16] Mobin, M. N., Haque, M. F. Re-strengthening of reinforced concrete (RC) beam using near surface mounted (NSM) steel re-bars. In: 4th International Conference on Civil Engineering for Sustainable Development; 2018; Khulna (BD). p.

[17] Sabah, S., Hamza, D. Flexural behavior of reinforced concrete beams strengthened with hybrid Steel-FRP reinforcements by using near surface mounted technique. Journal of Applied Engineering Science, 2023; 21: 1–9. doi:10.5937/jaes0-39645.

[18] Kholil, M., Shakib, S., Rakib, M., Morshed, A. Finite element modeling of RC beams retrofitted with near surface mounted steel bars. 2023; 21: 1–9. doi:10.1063/5.0130156.

[19] Olajumoke, A. M., Dundu, M. Methods for flexural strengthening of reinforced concrete elements using steel plates. In: International Conference on Construction Materials and Structures; 2014; Johannesburg, (ZA). p. 1080–1085.

[20] Abuodeh, O. R., Abdalla, J. A., Hawileh, R. A. The flexural behavior of bolting and bonding Aluminum Alloy plates to RC beams. Procedia Structural Integrity, 2019; 17: 395–402. doi:10.1016/j.prostr.2019.08.052.

[21] Zhang, Y., Wang, H., Qin, Y., Huang, S., Fan, W. Experimental and analytical studies on the flexural behavior of steel plate-UHPC composite strengthened RC beams. Engineering Structures, 2023; 283: 115834. doi:10.1016/j.engstruct.2023.115834.

[22] Looney, T. J. Bond behavior of high-volume fly ash and self-consolidating concrete [Master Thesis]. Rolla (MO): Missouri University of Science and Technology; 2012.

[23] American Concrete Institute (ACI). ACI 318-19: Building code requirements for structural concrete and commentary. Framington Hills (MI): ACI 318-19; 2019.

[24] American Concrete Institute (ACI). ACI 211-91: Standard Practice for Selecting Proportions for Normal, Heavyweight and Mass Concrete. Framington Hills (MI): ACI; 1991.

[25] ASTM International. ASTM A615/A615M-24: Standard Specification for Deformed and Plain Carbon-Steel Bars for Concrete Reinforcement. West Conshohocken (PA): ASTM International; 2024. doi:10.1520/A0615_A0615M-24

[26] ASTM International. ASTM A370-17: Standard test methods and definitions for mechanical testing of steel products. West Conshohocken (PA): ASTM International; 2017. doi:10.1520/A0370-17

[27] ASTM International. ASTM A36/A36M-19: Standard Specification for Carbon Structural Steel. West Conshohocken (PA): ASTM International; 2019. doi:10.1520/A0036_A0036M-19

[28] ASTM International. ASTM C39/C39M-24: Standard test method for compressive strength of cylindrical concrete specimens. West Conshohocken (PA): ASTM International; 2024. doi:10.1520/C0039_C0039M-24

[29] ASTM International. ASTM C496/C496M-17: Standard test method for splitting tensile strength of cylindrical concrete specimens. West Conshohocken (PA): ASTM International; 2017. doi:10.1520/C0496_C0496M-17

[30] ASTM International. ASTM C78/C78M-22: Standard test method for flexural strength of concrete. West Conshohocken (PA): ASTM International; 2022. doi:10.1520/C0078_C0078M-22.

[31] EFNARC. Specifications and Guidelines for Self-Compacting Concrete. Flums, (CH): EFNARC; 2002.

[32] Park, R. Evaluation of ductility of structures and structural assemblages from laboratory testing. Bulletin of the New Zealand Society for Earthquake Engineering, 1989; 22: 155–166. doi:10.5459/bnzsee.22.3.155-166.

[33] Kristiawan, S., Supriyadi, A., Sangadji, S., Santosa, D. Cracking behaviour and its effect on the deflection of patched-reinforced concrete beam under flexural loading. In: MATEC web of conferences; 2017; p. 02021. doi:10.1051/matecconf/201713802021.

[34] Porter, N. M., Stallings, J. M. Flexural strengthening of reinforced concrete beams with externally bonded CFRP plates with lap splices. Highway Research Center Auburn University; 2001. Report No.:1.

[35] Hamed, T., Said, A. Shear Strength and Serviceability of GFRP-Reinforced Concrete Beams: A Study on Varying Reinforcement Ratios. Civil Engineering Journal, 2025; 11: 857–883. doi:10.28991/CEJ-2025-011-03-04.

[36] Jomaah, M. M., Ghaidan, D. J. Energy Absorption Capacity Of Layered Lightweight Reinforced Concrete Beams With Openings In Web. Civil Engineering Journal, 2019; 5: 690–701. doi:10.28991/cej-2019-03091279.